Geological evolution of the mafic and felsic granulites from the central and northwestern parts of the Eastern Ghats Province in the context of Grenvillian-age tectonics

Summary by

Arnob Kumar Mondal

Registration no. – R-19RS215170198

Prof. Sankar Bose
(Supervisor)

Prof. Gautam Ghosh
(Co-supervisor)

2023

Introduction

Orthogneissic rocks (charnockite, granite gneiss and mafic granulite) are important constituents of the Earth's lower continental crust and they play important roles in orogenic processes. While mafic granulites are conceived as the major component of the deeper section of many regional granulite belts, granitic rocks typically expose at lower to mid-crustal levels. Charnockites are more akin to granites in occurrence, but they are mostly occurring in Precambrian terranes. Presence of charnockite in the Proterozoic lower crust, now represented as regional granulite terranes is well understood in the context of subduction-collision tectonics (Duchesne and Wilmart, 1997).

Mafic granulites either originate from crystallized mafic magma at deep crust (Huppart and Sparks, 1984) or dehydration melting of amphibolite facies middle crust (Brown, 1994). Relict textures often help in differentiating these two genetic types. While the former type helps in understanding the crust-mantle interaction in an orogenic lower crust, the latter type is a key marker for subduction-collision process in a thickened continental crust (Villaseca et al., 2022). If formed as mafic magma, such rocks have potential for supplying heat from the mantle. The volume of the rocks in such cases becomes important factor. Apart from deciphering the pressure and temperature conditions, mafic granulites can be studied to understand the fluid-rock interaction at deep crustal level. Oxide-sulphide phase relations (Fe-Ti oxides, Cu-Fe sulphides and graphite), in combination with silicate minerals in such rocks can help in elucidating the role of fluids in oxidizing and/or reducing large regions of lower crust during granulite facies metamorphism (Rollinson, 1980; Frost and Chacko, 1989).

Charnockites have been described in various ways in the literature. Frost and Frost (2008) clubbed all the felsic rocks containing orthopyroxene under the term "charnockite," irrespective of their origin. Thus, magmatic charnockites are typically anhydrous and are formed by the solidification of highly differentiated magma sourced from either the crust (Duchesne et al., 1989; Hughes et al, 2004) or mantle (Emslie et al., 1994) sources having crystallization temperature >900°C (Kilpatrick and Ellis, 1992; Percival and Mortensen, 2002; Mendes and De Campos, 2012). Yang and Santosh (2015) indicate that such rocks primarily originate from crystallized arc magmas, with only minor contributions from crustal components. As opposed to those formed by metamorphic (Newton et al., 1980) or anatectic (Bose et al., 2020) processes, magmatic charnockites occupy significant volume. Magmatic charnockite formed in a

convergent setting is typically distinguished by its high-pressure emplacement in the deep crust, which has a significant influence on granulite facies metamorphism (Frost et al., 2000; Frost and Frost, 2008). Often, they serve as heat sources for ultrahigh temperature (UHT) metamorphism (Schorn et al., 2020) as well as, in some cases it has been considered as a product of UHT metamorphism (Rajesh et al., 2014; Klaver et al., 2015). Magmatic charnockites such as the Mawson charnockite in East Antarctica (Young et al., 1997, Halpin et al., 2012) and unnamed charnockites in Peninsular India (Tomson et al., 2006, 2013; Rajesh, 2012; Gao et al., 2021) constitute regional granulite terrane. Rajesh (2012) suggests that these charnockites formed through arc accretion during significant orogenic events in two Proterozoic terranes of peninsular India: the Southern Granulite Terrain and the Eastern Ghats Belt.

Granitic rocks are integral part of orogenic belts and these rocks are formed by partial melting of metasediments, or, less likely by differentiation of basic magma. In regional granulite terranes, these rocks show a multitude of forms, like migmatitic gneiss, augen gneiss, or as highly deformed variety such as leptynite. Anatectic granites provide important clues to crustal differentiation process during major phase of orogeny and these rocks are often considered as the end product of orogenic cycle. Production of granitic rocks either by anatectic or magmatic process in an orogenic setting is a key to understand formation and evolution of continents at large (Condie, 2005). In regional granulite terranes, granitic rocks are often intimately associated with charnockite, and these two rocks are often considered as the differentiated products of same felsic magma under contrasting fluid regimes (Harlov et al., 2013).

Eastern Ghats Belt (EGB) of India (Fig. 1) is a regional granulite terrane where deep lower crustal section is exposed. Moreover, the evolution of this terrane is linked with the Proterozoic terranes of East Antarctica. Although orthogneissic rocks constitute the major part of the lithology of this terrane, these rocks are seldom studied. While the focus has been laid on paragneissic rocks to understand the metamorphic conditions (Bose, 2020 and references therein), very few studies have been carried out on mafic granulites (Dasgupta et al., 1991, 1993; Shaw et al., 1997; Bhui et al., 2007; Kelsey et al., 2017) or charnockite (Rajesh, 2014). From geochronological data, two major pulses of charnockite magmatism have been recorded in the EGB at ca. 1700-1600 Ma (Bose et al., 2011; Sarkar et al., 2015) and ca. 1000-950 Ma (Grew and Manton, 1986; Aftalion et al., 1988; Paul et al., 1990; Shaw et al., 1997; Krause et al., 2001). Despite the reported ages, no detailed geological investigation has been carried out, particularly on the charnockite and its associated rocks. This is a significant gap in knowledge since

charnockite and associated granites and mafic granulites are an integral lithological component of the terrane. A detailed investigation on these rock types would provide important clues regarding the metamorphism and tectonic history of the terrane during the period when India and East Antarctica had a shared geological history.

The present study is aimed to understand the geological evolution of the orthogneissic rocks from the central and northern regions of the EGB. It focuses on the granite, charnockite, and the mafic granulite, examining their field relationships, mineral evolution, geochemistry, geochronology, and silicate-oxide-sulphide mineral associations. Based on the magmatic and metamorphic history, the cratonization of the EGB along its margin can also be deciphered. The results of this study would help in understanding the magmatic/anatectic processes in an orogenic crust as well as interpreting the tectonic evolution of EGB in the context of India-East Antarctica correlation.

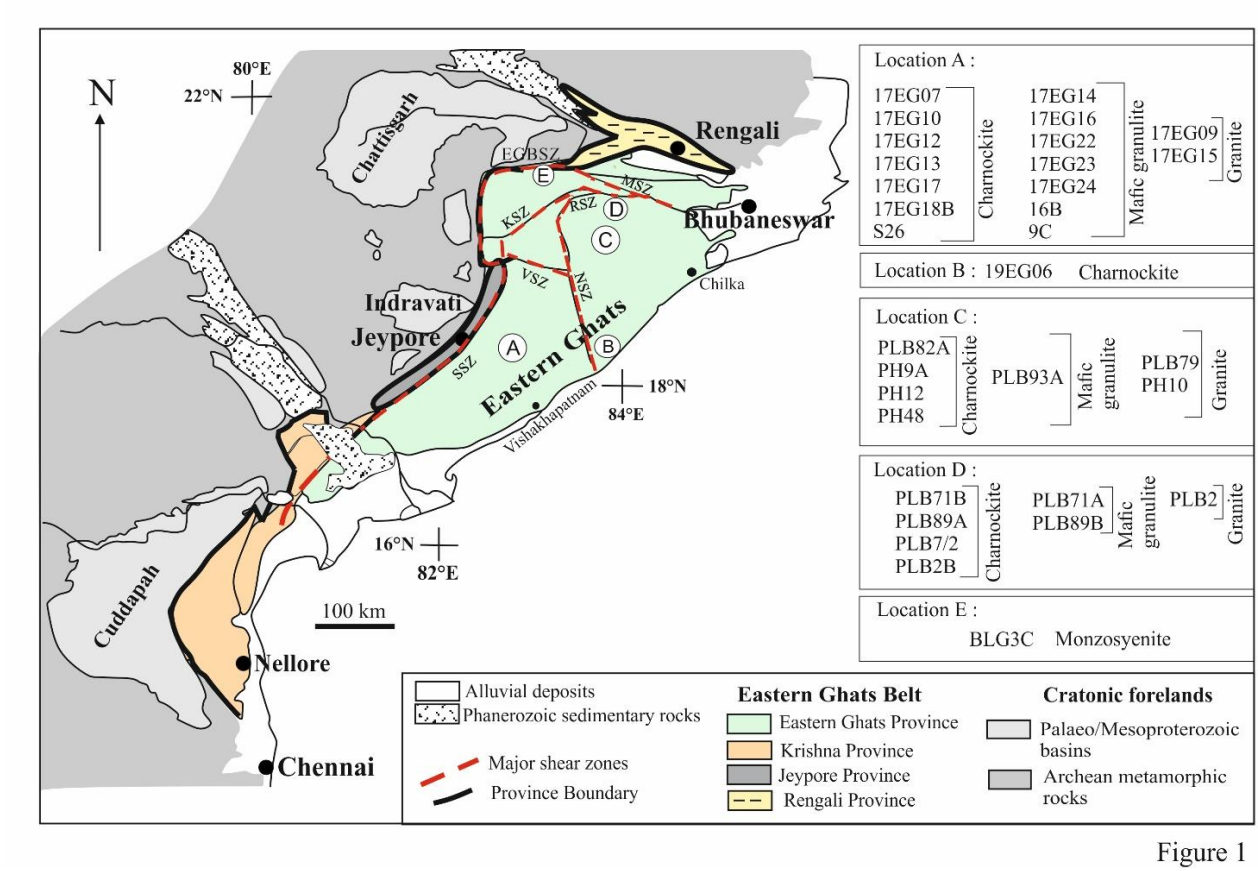

Figure 1

Fig. 1. General geological map of the EGB modified after Dobmeier and Raith (2003) showing sample locations within the Eastern Ghats Province (EGP). Abbreviations used are MSZ: Mahanadi Shear Zone, VSZ: Vamshadhara Shear Zone, NSZ: Nagavalli Shear Zone, SSZ: Sileru Shear Zone, RSZ: Ranipathar Shear Zone, KSZ: Koraput- Sonepur Shear Zone and EGBSZ: Eastern Ghats Boundary Shear Zone.

Geological background

Ramakrishnan et al. (1998) divided EGB into four longitudinal lithological zones. The Eastern and Western Khondalite Zones on two sides represent the paragneissic rocks, while the migmatite zone at the central part is composed mainly of felsic igneous rocks, namely charnockite and granite. EGB was later classified into four crustal domains based on isotopic signatures and large-scale structures by Rickers et al. (2001). Subsequently, Dobmeier and Raith (2003) subdivided the entire belt into four crustal provinces. The Krishna Province to the south consists of low- to medium-grade Udaygiri and Vinjamuru domains, and the high-grade Ongole domain of Paleo-Neoproterozoic age. The Jeypore Province to the west features high-grade mafic granulite and charnockite that may date back to the Neoarchean. The Eastern Ghats Province (EGP) at the center comprises various smaller crustal domains. The Rengali Province to the north is characterized by medium- to high-grade rocks of Meso-Neoarchean age (Bose et al. 2016). These four crustal provinces, with distinct isotopic signatures, exhibit distinct metamorphic features (Dasgupta et al., 2013, 2017; Bose and Dasgupta, 2018; Bose, 2020).

EGP underwent geological transformations in the time span of ca. 1200-500 Ma. High-grade granulite facies metamorphism has occurred at ca. 1030-990 Ma following a counterclockwise P-T path that culminated in ultrahigh temperatures (UHT; > 900°C) and significant partial melting and extraction of melt in the presence of CO_2-rich fluid during the metamorphic peak (Bose et al., 2009, 2016, 2020, 2022; Ganguly et al., 2017; Das et al., 2021). Recent research suggests that two distinct tectonometamorphic cycles occurred ca.1030-970 Ma and ca. 950-900 Ma (Bose et al, 2022) as opposed to a long-lived tectonics spanning ~180 Ma (Korhonen et al., 2013). The EGP's orogenic cycle, associated with the formation of supercontinent Rodinia, occurred around 1030-900 Ma and is thought to be part of a composite orogenic belt (R-EG) with the Rayner Province of East Antarctica (Mezger and Cosca, 1999; Upadhyay et al., 2009; Bose et al., 2011; Korhonen et al., 2013; Morissey et al., 2015; Dasgupta et al., 2017; Bose and Dasgupta, 2018). Orthogneissic rocks, including charnockites, are found extensively on both sides of the former R-EG. Notably, charnockite magmatism event occurred around 980-960 Ma during the period when the lower crust was recuperating from UHT metamorphism (Grew and Manton, 1986; Paul et al., 1990; Ganguly et al., 2018). Mafic granulites are interpreted as crystallized mafic magmas that was emplaced either at ca. 1450 Ma (Shaw et al., 1997) or at ca. 1560 Ma (Kelsey et al., 2017). Granitic magmatism in the EGP

occurred in the time frame ca. 980-940 Ma (Bose et al., 2011; Ganguly et al., 2018), which suggests these rocks are synchronous to charnockites in their magmatic histories.

Objectives

The identified objectives of the present work are given below.

1. To unravel the tectonometamorphic and geochronological history of the orthogneissic rocks of the EGP. This will help to identify the crustal growth history of the EGP.
2. To understand the juxtaposition of the EGP with the cratonic parts of India along the NW margin and the effect of hot orogeny on the colder cratonic lithosphere.
3. To understand the behaviour of deep crustal fluid during metamorphism on a regional and local scale. This will help in evaluating the effect of fluid on the stability of datable minerals (monazite, zircon).
4. To understand the geochemical evolution and paleotectonic settings of the orthogneisses (especially charnockite and mafic granulite), so that a model could be proposed and a proper correlation with its Antarctic counterpart could be made.

Lithology and sample description

The area chosen for the present study belongs to the central (Vishakapatnam domain) and northwestern (Phulbani domain) parts of the EGP. Pelitic migmatites and quartzofeldspathic gneisses (leptynite) dominate the central region, but charnockite, mafic granulite and khondalite also occur at places. Other paragneissic rocks like the calc-silicate granulite and aluminous granulite are sporadic in occurrence. Aluminous granulite and mafic granulite occur as enclaves within leptynite and locally charnockite. The gneissic foliation in the host leptynite is characterized by alternating garnet-biotite and quartzofeldspathic layers. In the Phulbani area, aluminous granulite and calc-silicate garnulite occur within felsic augen gneiss, while lenses of mafic granulites occur within coarse-grained charnockite (Ganguly et al., 2017). Two varieties of charnockites are reported from the EGP; one fine-grained foliated and the other coarse-grained massive. The former is more deformed along with the migmatitic felsic gneisses and aluminous granulite with a dominant E-W trending S_3 structure (Ganguly et al., 2021). The Araku-Anantagiri-Koraput areas of the Vishakhapatnam domain is dominated by khondalite and massif type coarse-grained charnockite (Fig. 1). The latter rock contains enclaves of aluminous

granulite, mafic granulite, calc-silicate granulite, and quartzofeldspathic gneiss. It forms extensive dome like outcrops, apparently massive with megacrystic feldspar laths (Fig. 2a). Such laths are mostly random in orientation, except in shear zones where they show augen structure. Plagioclase phenocrysts locally show orbicular structure (Fig. 2b). Based on the field evidences, this charnockite is characterized as magmatic one. In deformed samples, an imperfect gneissic foliation is created by alternating pyroxene-rich and quartzofeldspathic layers. Garnet grains can be found at the interface of plagioclase- and orthopyroxene-rich layers. The charnockite is locally affected by the D_4 event producing NW-SE trending S_4 foliation. Fifteen samples were collected from the two crustal domains of the EGP for the present study (Fig. 1).

Mafic granulite shows variable structure ranging from massive to crudely foliated, and occurs as enclave/xenoliths in coarse-grained charnockite. Out of the eight representative samples, one from the Chhatrang locality is mylonitized and hosted within felsic gneiss close to the Ranipathar shear zone (Fig. 1). In Koraput, the mafic granulites have a migmatitic appearance and contain an irregularly distributed leucosome layer in the form of patches and lenses up to 3 cm in width (Fig. 2c). The orientation of the foliation in the mafic granulites varies across the different locations, ranging from NE-SW to NW-SE and N-S.

Granites are similar in occurrence to the charnockite. They are generally medium to coarse-grained, with flat to boulder-type outcrops (Fig. 2d). The porphyritic nature is due to large clasts of feldspar. Garnet porphyroblast is sporadically present. Six representative granite samples were collected from various locations within EGP.

Apart from these, small outcrops of monzosyenitic rock are present along the north and northwestern margin of the EGP and these rocks have been studied to fix the time of final juxtaposition of EGP against cratonic India.

Methodology

Characterization of opaque minerals (oxide/sulphide) were done using Vega-Tescan scanning electron microscope and later using JEOL JSM IT500 scanning electron microscope at Presidency University and EDS data were acquired for spots to identify the elements within pyrite and pyrrhotite grains in different samples. Further, high resolution Backscatter electron (BSE) images were generated using the SEM and these images were used to select areas for chemical analysis by electron microprobe.

Figure 2

Fig. 2. Field photographs showing (a) randomly oriented plagioclase crystals within coarse-grained charnockite, (b) coarse-grained charnockite showing orbicular plagioclase crystals, (c) migmatitic mafic granulite showing alternate layers of leucosome and melanosome, and (d) bouldery outcrop of porphyroblastic granite.

Chemical compositions of oxide and silicate minerals from mafic granulite samples were done using a CAMECA SX100 electron microprobe (EPMA) at the Indian Institute of Technology, Kharagpur, India. The instrument was operated at 15 kV acceleration voltage using 12 nA current and 1 μm beam diameter was used for the point analyses. Natural silicate and oxide standards were used for calibration, except for Ti and Mn (synthetic standard material used). The chemical analyses of charnockite samples were done with a Cameca SX Five Tactis EPMA at the National Centre for Earth Science Studies (NCESS), India. The instrument was operated with 15 kV accelerating voltage, 20 nA beam current, and 1 μm beam diameter.

For whole rock chemistry, representative samples were crushed using a jaw crusher followed by pulverizer (Fritsch) at the Presidency University. Major and trace elements of 12 representative samples of charnockite were analyzed at the NCESS. Major elements were analyzed using WD-XRF (Bruker S8 Tiger sequential WD X-ray spectrometer) using pressed pellets. The standards used were BHV01, G2, GSN and W2a. Analyses for rare earth elements

(REE) of the charnockite samples were done at the M/s Acme Laboratory, Vancouver, Canada (Bureau Veritas Commodities Canada ltd), with the litho-geochemistry package LF100 for measurement of selected trace and REE concentration using the STD-SO-19 reference material. Samples of granites and mafic garnulites were analyzed at the ALS laboratory and University of Rochester for whole rock chemical analysis.

For zircon U-Pb geochronological analysis, about 2 kilograms of representative charnockite and mafic granulite samples were manually crushed for zircon U-Pb analyses using an agate ball mill (Fritsch Pulverisette 0). The powdered samples were collected using disposable sieve cloth and further processed in water and the heavy minerals were separated manually. Careful attention is paid to avoid possible cross-contamination. Zircon grains were then handpicked from each heavy mineral separate and mounted onto a standard epoxy disc with a diameter of 25 mm. Each mount was polished until the maximum surface areas of the zircon grains were exposed. The internal structures of these grains were examined by cathodo-luminescence (CL) and BSE imaging using the Cameca SX Five Tactics EPMA at NCESS. Single spot U-Pb isotope and trace element analyses of zircons were conducted at the Isotope Geochemistry Facility at NCESS, using a Teledyne CETAC, Nd: YAG (213 nm) solid-state laser coupled with Agilent 7800 quadrupole ICP-MS. All errors are reported in 2σ confidence.

Results

Petrography and mineral chemistry

Coarse-grained charnockite: The charnockite samples display broadly similar mineralogy and texture, but variations exist among the samples. While all the samples have undergone high-temperature metamorphism, some have undergone intense recrystallization during ductile shearing, while others have preserved relict magmatic textures. The mineral assemblage consists of orthopyroxene (Opx), plagioclase (Pl), K-feldspar (Kfs), quartz (Qtz), ilmenite (Ilm), apatite (Ap), and biotite (Bt), along with garnet (Grt), clinopyroxene (Cpx), hornblende (Hbl), magnetite (Mag), zircon (Zrn), pyrrhotite (Po), and chalcopyrite (Cp). Based on the presence of Grt, the rock has been subdivided into two types. In Grt-bearing charnockite, the gneissic foliation is characterized by alternating layers of Opx (+ Grt)-bearing and quartzofeldspathic layers. Grt occurs either as porphyroblast (Grt_1; $Alm_{66–76}Prp_{9–14}Grs_{7–22}$) typically surrounded by a thin collar of Qtz and Kfs or as corona with Qtz (Grt_2; $Alm_{64–72}Prp_{8–25}Grs_{6–21}$) on Ilm and Opx ($X_{Mg}$ -

0.42–0.59) (Fig. 3a). Bt (X_{Mg} -0.40–0.87) partially replaces Opx and Grt, while Hbl (X_{Mg} = 0.42–0.46) partially replaces Cpx in one sample. Kfs and Ilm form symplectic intergrowths at the margin of Bt (Fig. 3b). Perthitic Kfs ($Or_{96–97}Ab_{3–4}$ to $Or_{77–81}Ab_{19–23}$) contain pockets of Qtz and develop myrmekitic textures along the grain boundaries. Deformation is indicated by undulose extinction, dynamic recrystallization, and subgrain formation in Qtz, Opx, and feldspar. In a sample from the Ranipathar shear zone, all the phases show evidence of stretching along the foliation. The Grt-absent charnockite locally show orbicular structure (Fig. 2b), where megacrystic Pl grains (up to 6 cm in length) occur in an Opx-Pl-Qtz matrix. Porphyroblastic Opx grains are marginally overprinted by Bt + Qtz intergrowth. The presence of cuspate grain boundaries between Qtz and feldspar grains potentially suggests crystallization in the presence of melt. Evidence of deformation is demonstrated by the occurrence of Qtz ribbons, recrystallization of Qtz, feldspars, and Opx, deformation twinning in Pl, and kink bands in Bt.

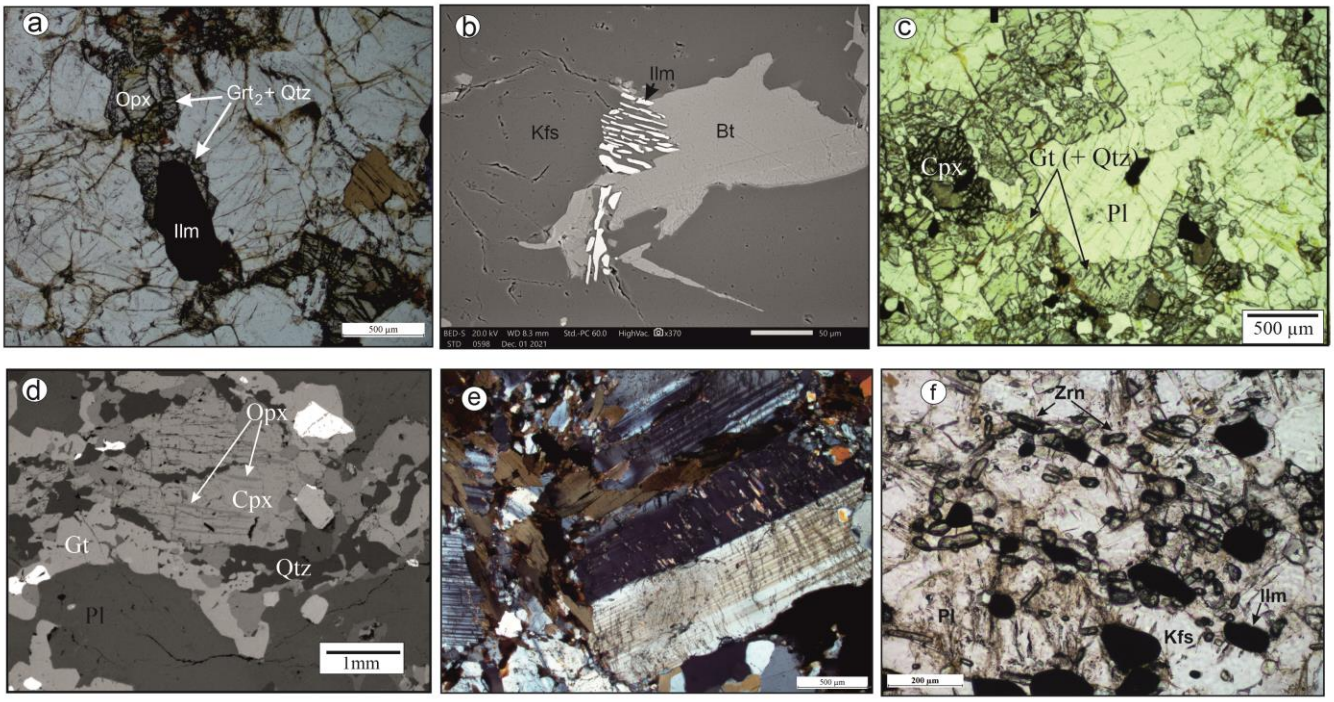

Figure 3

Fig.3. Photomicrographs and Back- Scattered Electron (BSE) images. (a) Garnet (Grt2) corona on porphyroblastic orthopyroxene (Opx) and ilmenite (Ilm) in massif type charnockite. (b) Partial breakdown of biotite (Bt) to a skeletal intergrowth of K-feldspar and ilmenite (Kfs+Ilm) in charnockite. (c) Garnet (Gt) corona along with quartz (Qtz) around clinopyroxene (Cpx) in mafic granulite (d) Mafic granulite showing porphyroblastic clinopyroxene (Cpx) that contains exsolved lamellae of orthopyroxene (Opx). (e) Blastoporphyritic plagioclase (Plg) grains in granite. (f) Zircon (Zrn) and ilmenite (Ilm) withn Kfs + Plg matrix in monzosyenite.

Mafic granulite: Mafic granulites are also subdivided into two assemblages based on presence of Grt. The Grt-absent assemblage is consisted of Opx, Cpx, Pl, Kfs, Hbl, Bt, Ilm, Ap, Mag and sulphide phases. Mag occurs in different modes, including oxide phases within porphyroblasts (Mag_1), as discrete grains (Mag_2), Mag_3 with Py_2 replacing Po, and as fracture filling in veins (Mag_4). In general, all the samples exhibit a granoblastic texture. Both Opx (X_{Mg} = 0.53–0.55) and Cpx (X_{Mg} = 0.70) contain exsolved lamellae while Ilm_2 grains mostly free of it. Pl (X_{An} = 0.73) show deformed twin lamellae and Kfs patch. Ilm_2 (X_{Haem} = 0.05, 0.87-1.12 wt.% BaO) grains (>400μm in size) are found adjacent to porphyroblastic Opx and Cpx. Hbl occurs as patches on porphyroblastic Opx (X_{Mg} =0.61). Along the grain boundaries of Bt and porphyroblastic Hbl, minute recrystallized orthopyroxene grains are present. The leucosome layer contains cuspate grains of quartz and feldspar. The Grt-bearing mafic granulite additionally contains Grt with Py, Po and small amount of barite and calcite. Grt is either porphyroblastic ($Alm_{58–59}Prp_{18–19}Grs_{18–19}Sps_{2–3}$) or coronal ($Alm_{58–60}Prp_{16–19}Grs_{17–19}Sps_2$) with or without intergrown Qtz separating porphyroblastic Opx and Cpx (X_{Mg} =0.71–0.77) from Pl ($Ab_{42–59}An_{39–52}Or_{1–2}$) (Fig 3c). Evidence of grain-scale deformation is evident from recrystallization, formation of Qtz ribbon and stretched porphyroblasts. Cpx grains have exsolved lamellae of Opx (Fig. 3d). Vermicular Intergrowth of Qtz within Grt is common feature.

Granite gneiss and monzosyenite: These rocks are porphyritic in nature and have similar mineralogy and textural characteristics. The major phases include Grt, Qtz, Pl, Kfs, Bt, and Ilm, along with accessory minerals such as Ap, Zrn, and Mnz. It is common to find enclaves of pelitic granulite within these granites. The samples contain idioblastic to sub-idioblastic Grt porphyroblasts with inclusions of Qtz, Bt, and Ilm. These porphyroblasts show symplectic overgrowth of Bt + Qtz along the margins. The sample collected from the Tumudibandh area has both porphyroblastic and matrix Grt. The rock commonly exhibits a granoblastic texture, where large Pl grains preserve relic igneous texture (Fig. 3e). Feldspar often form subgrains along the margins and are recrystallized, while both feldspars and Qtz show undulose extinction while Bt exhibits kinking. Samples collected close to the Ranipathar shear zone are mylonitized, and preserve well developed Qtz ribbons. The foliation wrapping porphyroblastic grains locally shows symmetric/asymmetric tails.

The monzosyenite vein intrudes the felsic gneiss (granite gneiss) country of the Bolangir anorthosite massif. The felsic gneiss shows a strong N-S trending gneissic foliation which is cut by the vein. The rock is finer-grained, mostly recrystallized and greyish in colour. It contains abundant Pl with Qtz with relatively rare Kfs. Bt flakes locally show a crude foliation. A notable feature of the rock is the presence of Zrn + Ilm-rich layer (Fig. 3f) which appears to have developed during magmatic crystallization.

Geothermobarometry and phase diagram modelling

Conventional geothermobarometers were used to determine the P-T of metamorphism for the orthogneissic rocks. For the coarse-grained charnockite, Grt-Opx thermometer yielded a temperature range of 722-790°C at an assumed pressure of 8 kbar, while the GOPQ thermobarometer yields pressure range of 7.30-9.03 kbar and temperature range of 741-910°C for various samples. Additionally, the Ti-in zircon trace element thermometry was used based on the model of Ferry and Watson (2007). The crystallization temperature for different samples range from 660-862ºC, while the metamorphic temperatures calculated using Ti contents in zircon overgrowths and patches varied from 635-812ºC.

The peak metamorphic temperature of mafic granulite was estimated using fossil thermometers. The two-feldspar thermometer estimated a temperature of around 870°C, while the Opx-Ilm thermometer yields temperature of 890°C. The P–T conditions for the Grt-bearing assemblage were also determined. The GCPQ gives 7.5 kbar pressure while the Opx-Ilm thermometer gives 780°C. The Grt-Opx thermometer gives maximum temperature of 740°C, and the GOPQ barometer yielded pressure estimates of 7.7–7.9 kbar. The Grt-Cpx thermometer yields a maximum temperature of 830°C.

The pre-metamorphic evolution of coarse-grained charnockite was modelled using Perple_X 6.9.0 program at temperature (600-1200°C) and pressure (6-11 kbar) to examine the possible origin of the magma from hydrated basalt or amphibolite protolith in lower crustal conditions. As a possible protolith, hydrated basaltic bulk composition of the East Dharwar Craton has been used and phase diagrams were calculated using nine different bulk compositions in the NCKFMASHT system. The influence of CO_2-rich fluid by assigning hypothetical values of 0.7 wt.% H_2O and 0.3 wt.% CO_2 in the fluid mixture. At 8 kbar pressure and 900°C temperature, the resulting melt can contain up to 11% with over 60 wt.% of SiO_2. Increasing the temperature to 1000°C at the same pressure produces up to 25% melt with SiO_2 content ranging

from 52-56 wt.%. The melt compositions were compared using a TAS diagram, revealing that at 900°C, they fall within the quartz monzonite field, while at 1000°C, the Na_2O and K_2O contents are relatively higher and the compositions fall within the monzodiorite to monzonite fields. Although these values do not match exactly, the hypothetical melt and charnockite magma compositions exhibit a similar trend in the TAS diagram, possibly indicating some degree of crustal contamination of the magma.

Oxygen fugacity

Oxygen fugacity for the metamorphic assemblages of mafic granulite was determined using the QUILF program (Andersen et al. 1993). To ensure accuracy, precise temperature values and a fixed pressure of 8 kbar were used, based on estimates and previously published P-T records of mafic granulites (Dasgupta et al. 1993; Bose et al. 2000, 2003). The fO_2 value was determined by examining the reactions involving coexisting Opx-Ilm, Mag-Hem, and Opx-Mag-Qtz mineral pairs. The calculated fO_2 values from various reactions for were 3-4 log units higher than the FMQ equilibrium. Other samples exhibited low oxygen fugacity below the FMQ buffer, but showed textural evidence indicating an increase in fO_2, except for one sample. Pyrite was the dominant mineral over pyrrhotite in some samples, but Py and Mag replace pyrrhotite in other samples. As pyrrhotite is stable in a comparatively reduced condition, there must be a decrease in oxygen fugacity during the peak stage. The rocks experienced higher fO_2 during retrogression, which promoted the formation of Py and Mag replacing the pyrrhotite.

Geochemistry of charnockite

The SiO_2 content varies widely and has been grouped into high-SiO_2 and low-SiO_2 varieties. FeO_T and MgO exhibit wide variation (3.07-11.07 wt.% and 0.56-8.35 wt.% respectively), while CaO (2.81-5.8 wt.%) and K_2O (1.36-5.14 wt.%) vary considerably. LOI values (< 1 wt.%) indicate dry nature of mineral assemblages. To characterize the evolution and paleotectonic setting of the charnockite magma, only REE plots were used as reliable indicators. The samples are of intermediate variety in the SiO_2-Fe* plot and show overlapping distribution between I- and S-type granitoids. The extended trace element plot normalized to MORB (Sun and McDonough, 1989) shows enrichment of Rb, Th, K, Nd, Zr, and Hf, and depletion of Nb, Sr, Ta, P, and Ti (Fig. 4a). The samples have low Sr and high Y content, resulting in low-Sr/Y ratios, except for three samples that show Archean high-Al TTG affinity. Majority of the samples have Rb/Sr

greater than the mantle value, indicating upper crustal signatures. The Nb/Zr vs Zr plot suggests a collisional setting for both types of charnockite, while the La/Yb vs. Nb/La plot indicates an alkaline arc setting (fig. 4b). The REE plot normalized to chondrite values after McDonough and Sun (1995) exhibits patterns of high fractionation that are distinguished by an abundance of LREE in comparison to HREE (Fig. 4c). This is also indicated by high values of La/Yb_{CN} (ranging from 1.54 to 9.68, with an average of 5.0). Conversely, the HREE fractionation exhibits a nearly flat trend with depleted values of Ta/Yb_{CN}. The majority of the samples demonstrate a negative Eu anomaly (Eu/Eu* = 0.4 to 1.5, with an average of 0.66).

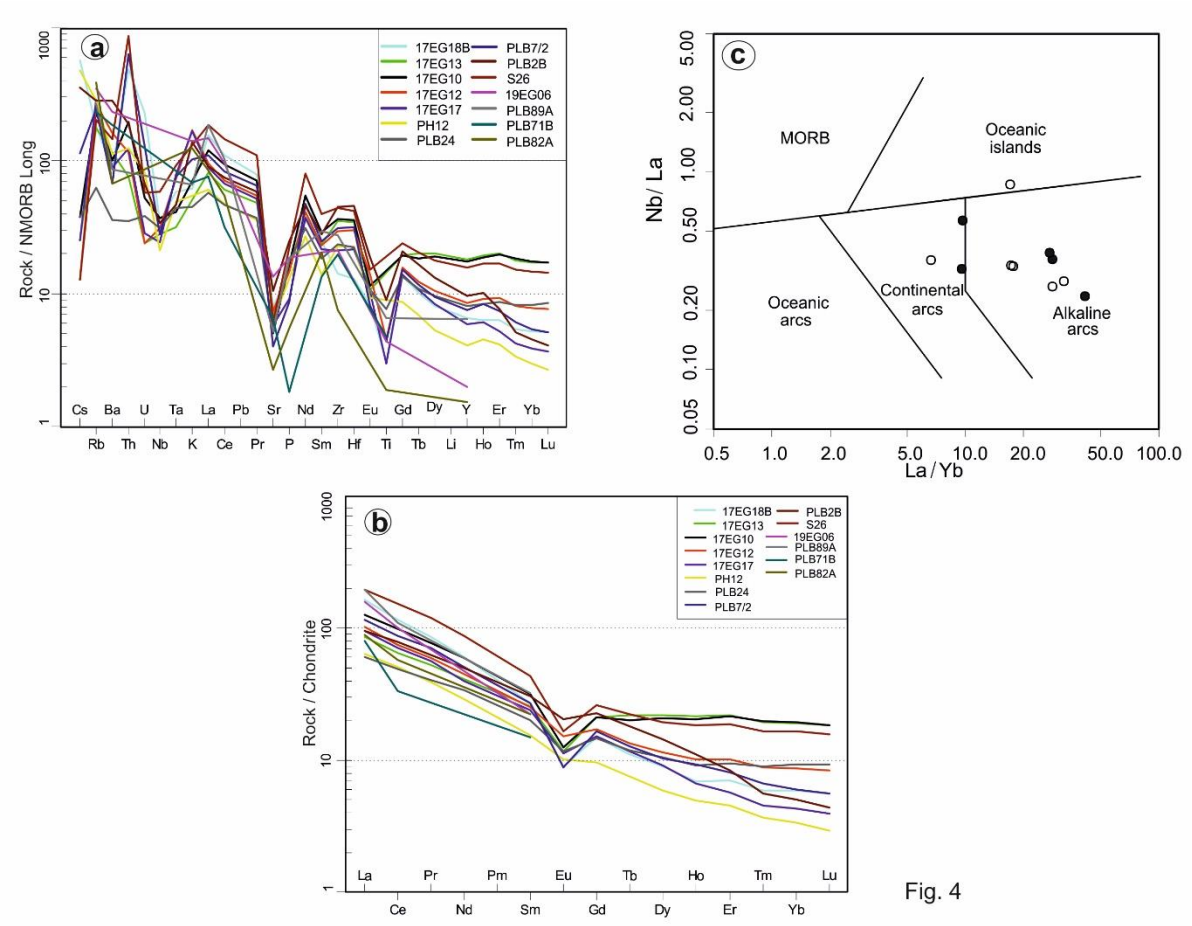

Fig. 4

Fig.4. Multiple plots of geochemical data of the coarse-grained charnockite. (a) Multi-element variation diagram for trace elements and REE of 14 samples normalized to MORB (after Sun and McDonough, 1989). Note the strong positive anomalies of Th, La, Ce and Nd while strong negative anomalies are found for Nb, P, Sr and Ti. (b) Nb/La vs. La/Yb plot of the same samples after Hollocher et al. (2012). Note the samples plot in the fields of alkaline arc to continental arc. (c) Chondrite-normalized REE plot (after McDonough and Sun, 1995) of the samples showing strongly fractionated REE patterns with a prominent negative Eu anomaly.

Geochemistry of granite

The granite shows a comparable geochemical composition to charnockite, with a wide range of SiO_2 (56.7-75.6 wt.%), FeO_T (0.98-7.95 wt.%), and MgO (0.07-1.9 wt.%). They are predominantly peraluminous, indicating enrichment in light rare earth elements (LREE) and depletion in heavy rare earth elements (HREE), with a negative Eu (Eu/Eu*= 0.39) anomaly. The trace element diagram illustrates pronounced negative anomalies for Sr and Ti and positive anomaly for Pb. In addition, there are weak negative anomalies for Ba, Ta, P, and weak positive anomalies for Th and Nd, and a flat trend for Zr-Hf is also noted.

Geochronology

Charnockite: The majority of the grains exhibit a thick internal domain with well-defined oscillatory zoning, which is surrounded by a thinner, featureless, or occasionally sector-zoned overgrowth with a thickness of 20-30 µm. Some grains exhibit xenocrystic cores. In *Sample 17EG07*, six spots from oscillatory domain yielded a weighted mean $^{206}Pb/^{238}U$ age of 939±27 Ma (MSWD=2.8; Fig. 5a). In *Sample 17EG10*, eight grains from the oscillatory-zoned domain yield a weighted mean $^{206}Pb/^{238}U$ age of 1002±13 Ma (MSWD= 1.2; Fig. 5b). Two spots from the overgrowth domain yield $^{206}Pb/^{238}U$ dates of 803±24 Ma and 886±18 Ma. In *Sample 17EG17*, nine spots from these domains yield a weighted mean $^{206}Pb/^{238}U$ age of 951±9 Ma (MSWD= 1.4; Fig. 5c). Analyses from overgrowth domains yield $^{206}Pb/^{238}U$ dates in the range of ca. 931–819 Ma. In *Sample PH9A*, ten analyses from the oscillatory-zoned domain yield a mean $^{206}Pb/^{238}U$ age of 1020±16 Ma (MSWD= 1.5; Fig. 5d). Analyses of overgrowth yield $^{206}Pb/^{238}U$ dates in the range ca. 949–927 Ma. In *Sample 19EG06*, nine grains form these group yield a weighted $^{206}Pb/^{238}U$ mean age of 954±8 Ma (MSWD= 1.01; Fig. 5e). Analyses from the overgrowth and patchy domains show $^{206}Pb/^{238}U$ dates in the range ca. 909–871 Ma. In *Sample PLB71B*, ten spots from this domain yield a weighted mean $^{206}Pb/^{238}U$ age of 951±13 Ma (MSWD=1.3; Fig. 5f). The two xenocrystic cores yield $^{206}Pb/^{238}U$ dates of 1039±28 Ma and 1156±23Ma dates, respectively. In *Sample PLB82A*, eight analyses from the oscillatory-zoned domains yield a weighted mean $^{206}Pb/^{238}U$ age 968±22 Ma (MSWD= 5.0; Fig. 5g). Spots from these domains yield $^{206}Pb/^{238}U$ dates in the range 925–813 Ma. In *Sample PLB89A* ten analyses from the same domains yield a weighted mean $^{206}Pb/^{238}U$ age of 978±16 Ma (MSWD= 3.2; Fig. 5h). Analyses on overgrowths yield $^{206}Pb/^{238}U$ dates in the range ca. 915–859 Ma.

Monzosyenite vein: Zircon grains in this are mostly elongated with a high aspect ratio (up to 3.0). These grains have prismatic to oval in cross-section. Most of the grains are 100-150 μm in length and their width varies from 30 to 50 μm. Almost all the grains show a uniform internal structure with a dark-CL central part surrounded by a light-CL exterior part. The latter domains show planar to faint oscillatory zoning. A total of 28 spots were analyzed from the same number of grains, out of which 21 near-concordant data yield a weighted average of $^{206}Pb/^{238}U$ dates of 490±3 Ma (MSWD = 1.03; Fig. 5i). The probability density plot of all the data shows a sharp peak at ca. 490 Ma. From the data, it is clear that the ca. 490 Ma is the age of intrusion of the monzosyenite vein.

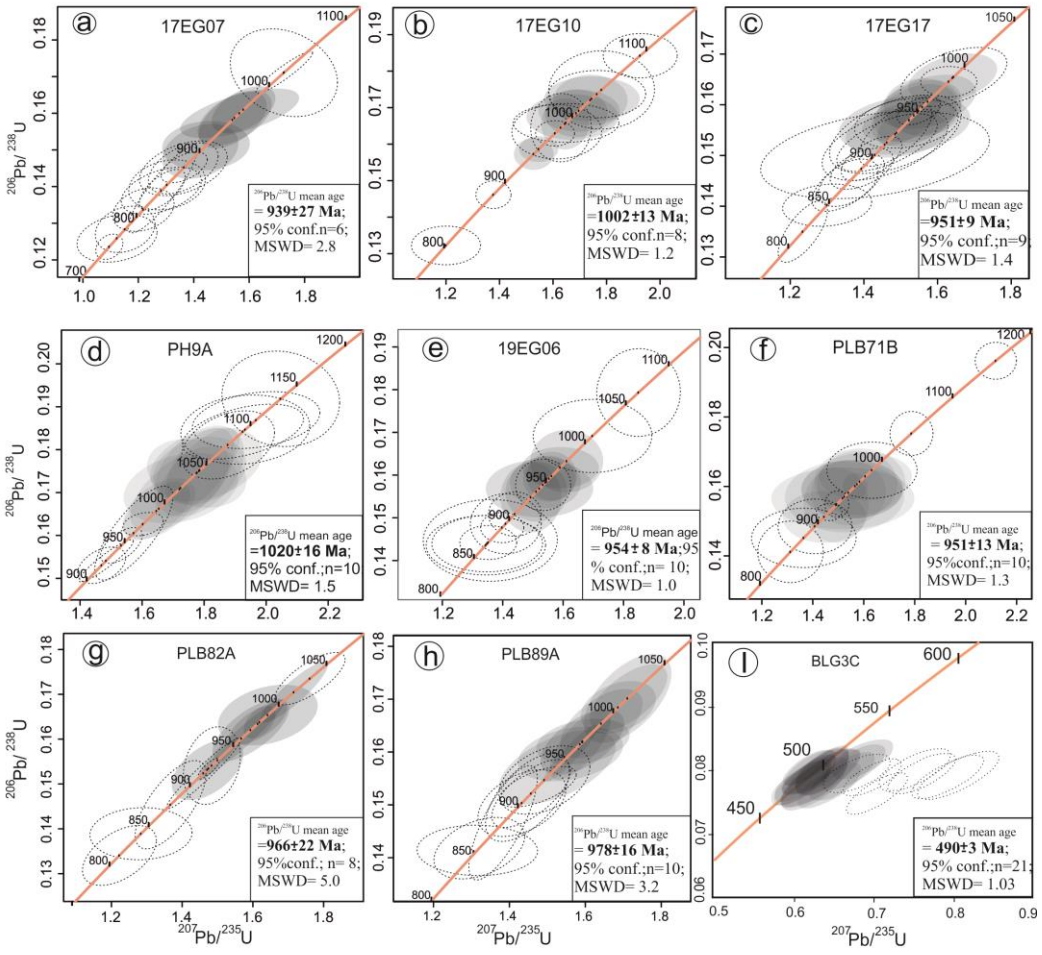

Fig. 5

Fig.5. Wetherill concordia plots for analyzed zircon grains from the studied charnockite samples. $^{206}Pb/^{238}U$ weighted average age for group of data showing oscillatory zoning is shown for each sample. (a) Sample 17EG07. (b) Sample 17EG10. (c) Sample 17EG17. (d) Sample PH9A, (e) Sample 19EG06. (f) Sample PLB71B. (g) SamplePLB82A. (h) Sample PLB89A (i) Sample BLG3C. For each sample, all data are plotted. Those used for group age calculations are shown as grey filled ellipses, while rest of the data are presented as open stippled ellipses.

Zircon trace element and REE chemistry of charnockite

Trace and REE chemistry of zircon was used to understand the geochemical characteristics of the oscillatory-zoned zircon domain. The U/Yb vs. Hf plots indicated continental arc signatures, with average U/Yb ratios suggesting a continental arc affinity, and higher values indicating possible contamination by mature, LILE-enriched crustal components. The U/Nb vs. Th/Nb plots showed high U/Nb and Th/Nb ratios, typical of an arc setting. The positive correlation of Yb and Ti rules out the role of amphibole and a positive correlation of Ti and the Gd/Yb ratio suggests early fractionation of titanite and apatite from the magma (Grimes et al. 2007, 2015). The compositions of the zircon population were compared with those of known provenance after Grimes et al. (2015). The oscillatory-zoned zircon shows positive anomalies of U and Th and negative anomalies of Eu and Ti, with weak positive anomalies for Ce, Dy, and Sm, and weak negative anomalies of Pr and Nd. The zircon exhibited a depletion of LREE and an enrichment of HREE, typical of igneous zircon crystallized from granitoid magma (Hoskin and Black, 2002 and Belousova et al. 2002). The trace element and REE patterns of the zircon overgrowth and patches overlap with those of the magmatic zircons, but exhibited more fractionated patterns with a slight depletion of LREE, a concave up distribution of HREE from Gd to Er, and a flat distribution from Er to Lu. Ti indicated a strong negative anomaly among the HFSE.

Discussion

Evolution of the massif type charnockite and granite of the EGP

Extensive area of EGP contains charnockite in association with pyroxene-free granitoids (granite), khondalite, and calc-silicate granulites. The geological relationships in the field reveal that the charnockite magma has intruded the sedimentary rocks, which have undergone UHT metamorphism between ca.1030 to 990 Ma. Additionally, charnockite contains enclaves of these sedimentary rocks (Ganguly et al., 2017). From structural data, the emplacement of charnockite magma has been constrained as post-D_2/D_3 (Ganguly et al., 2018, 2021). These rocks are typical granulites with varying compositions due to magmatic differentiation and potential crustal contamination. Most have a granoblastic texture with some degree of metamorphic recrystallization, although weak foliation can be observed, particularly near ductile shear zones, where tailed porphyroclasts and feldspar augen are present. Primary igneous textures are still evident, despite high-temperature metamorphism. Textural evidence suggests a retrogressive

change during cooling like the Grt corona on Ilm and Opx, and the breakdown of Grt to Bt + Qtz symplectite. Presence of Grt as a primary phase implies its crystallization from the primary magma. Maximum P-T during this stage is estimated to be 910°C/9 kbar. Textures like the breakdown of biotite to a symplectic intergrowth of Ilm + Kfs suggests an event of incipient heating of the already cooled crust that implies that the cooled charnockite magma experienced reworking possibly related to the M_2 cycle of metamorphism (ca. 950-900 Ma). Charnockite magma was mostly dry, but coeval granite magmatism (Bose et al., 2011) in the EGP implies a fluctuation of the fluid regime in terms of CO_2-H_2O components (Harlov et al., 2013). The charnockite rocks display metaluminous to weakly peraluminous traits and have a calcic, alkali-calcic, or alkalic nature which is similar to its counterpart Mawson Charnockites and northern Prince Charles Mountain (nPCM). The rocks exhibit LREE enrichment and depleted in HREE, with elevated Ba contents and positive anomalies of Pb, La, Nd, and Gd, as well as negative anomalies of Nb, Ta, Sr, and Ti, with slightly negative Ce and Y anomalies, which suggests an arc setting (Yang et al., 2016; Hollocher et al., 2012). Rb and K enrichment may be associated with an increase in the percentage of alkali elements. The significant differentiation of the magma likely resulted in Zr and Hf enrichments. The origin of the parent rock that generates charnockite magma is a contentious topic (Frost and Frost, 2008); however, theoretical modeling on partial melting of hydrated basaltic rock under carbonic fluid regime provides a plausible explanation for the generation of charnockite magma in a subduction setting. Zircon U-Pb data shows two periods of charnockite magma crystallization: two samples crystallized around 1020-1000 Ma, while the remaining six crystallized around 980-940 Ma. This suggests a 40-million-year gap between two charnockite magmatism occurrences in the EGP. The timing of the first pulse closely coincided with UHT metamorphism, whereas the second and final pulse took place between the M_1 and M_2 cycles of metamorphism (Bose et al., 2022). The latter event occurred when the lower crust was recuperating from UHT metamorphism. Zircon data obtained from the overgrowth and patchy domains reveal nearly concordant spot dates within ca. 950-750 Ma. This could be linked to subsequent metamorphism (M_2: approximately 950-900 Ma, Bose et al., 2022) and/or modifications caused by fluids (approximately 550-500 Ma, Das et al., 2021). Trace and REE data from different zircon domains show unique patterns. They are depleted in LREEs but enriched in HREEs, display negative Eu and Ti anomalies. These features suggest that the magma originated in the lower crustal level and underwent fractionation of plagioclase and Fe-Ti oxides (Belousova et al., 2002).

Mafic magmatism in the EGP

The Grt-free mafic granulites were produced from a mafic magmatic protolith that underwent metamorphism at a deep crustal level, leading to UHT conditions (Dasgupta et al. 1993; Sengupta et al. 1996; Bose et al. 2003; Bhui et al. 2007). The studied mafic granulite is formed by similar evolutionary process. Shaw et al. (1997) presented geochronological evidence that mafic magma intruded the lower crust around 1450 Ma in the Rayagada region of the EGP. Similarly, the Anakapalle locality of the EGP reported emplacement of mafic magma around ca. 1580 Ma (Kelsey et al., 2017). Recent tectonic modeling suggests that the metamorphism of the EGP took place in an accretionary tectonic setting, coinciding with rifting and the opening of the back arc basin (Dasgupta et al. 2013, 2017; Bose and Dasgupta, 2018). The sediments that were deposited within the back arc basin along with the mafic and alkaline magma (emplaced at ca. 1.48–1.30 Ga, Upadhyay 2008; Ranjan et al. 2018) and suffered UHT metamorphism along an anticlockwise path during 1030–990 Ma (Bose et al. 2011; Das et al. 2011; Korhonen et al., 2013b). This anticlockwise path possibly indicates significant magmatic activity during or after tectonic crustal thinning (magmatic intra or under-plating), which is typical of a magmatic arc (Abati et al., 2003). Migmatitic mafic granulite is less abundant in the EGP, so its history is not clear. It is formed from the anatexis of a mafic protolith, a process seen in other metamorphic terranes (Brown, 1994; Dziggel et al., 2012; Feisel et al., 2018). Experimental data shows that mafic protolith melts at temperatures above 800°C, with more than 10% of the melt produced at temperatures over 850°C, under pressures ranging from 5-10 kbar (Beard and Lofgren, 1991; Rushmer, 1991; Pati˜noDouce and Beard, 1995; L´opez and Castro, 2001). Conventional thermobarometric data suggests the peak metamorphic temperature at 8 kbar pressure was close to 890°C, but this may be a reset value since mafic granulites from nearby locations indicate higher temperature estimates (Dasgupta et al. 1991, 1993; Bose et al. 2003). Additionally, presence of orthopyroxene lamellae within clinopyroxene in the studied samples provides fossil evidence of UHT metamorphism (Frost and Chacko, 1989; Harley, 2008).

Fluid evolution at the lower crust

Textural analysis of mafic granulite indicates stability of Cpx, Opx, Pl, Ilm, Grt along with Mag, and sulphide phases (Po, Cp, and Py). Based on the pyrrhotite composition fS_2 value of −3.50 to −3.67 has been estimated. Temperature vs. fO_2 plot reveals lower fO_2 values for pyrrhotite-bearing assemblages compared to pyrite-bearing ones. Experimental data shows that in mafic

rock, sulphide phase stability depends on fO_2 conditions above 743°C, where pyrrhotite prevails over pyrite, regardless of fO_2 values (Kullerud, 1957). Pyrrhotite is the stable phase at the UHT metamorphic peak in both assemblages, whereas pyrite formed at lower temperatures. The pyrite-dominated assemblages have calculated fO_2 values 3-4 log units higher than the FMQ buffer. Pyrite and magnetite developed during the retrograde stage due to cooling under high fO_2 conditions.

The consistent high fO_2 condition in the mafic lower crust may be linked to the composition of the lower crustal fluid. While CO_2 and H_2O may not be particularly effective as oxidizing agents in rocks without graphite (Frost, 1991), it's possible that the SO_2 component found in brine could play a significant role in oxidation (Crawford and Hollister, 1986; Harlov et al., 1997; Newton and Manning, 2005; Harlov, 2012). In a subduction-accretion environment, fluids containing H_2O, Ca, and Al solutes are generated through subduction zone dehydration (Manning, 2004; Zheng et al., 2016). The resulting hydrothermal supercritical fluid is ideal for transporting sulphates due to the presence of alkali chloride components within it (Keppler, 1996; Ni et al., 2017; Barnes et al., 2018). Although brine-rich fluid inclusions are present in lower crustal rocks, they are not commonly observed due to their wetting behavior with mineral phases (Touret, 1985; Watson and Brenan, 1987; Manning and Aranovich, 2014). However, fluid inclusion data from various locations show evidence of CO_2–H_2O fluid species without any direct evidence for brine (Bose et al., 2016, 2009; Mohan et al., 2003; Sarkar et al., 2003). High F contents in fluor-biotite and fluor-wagnerite in mineral assemblages suggest the possible association of halogen-rich fluid species during metamorphic stages (Bose et al., 2005; Ganguly et al., 2017; Das et al., 2017). Brine composition varies with rock type, with NaCl dominating in granitic rocks and $CaCl_2$ dominating in mafic rocks (Moller et al., 1997; Stober and Bucher, 2005).

Juxtaposition of EGP against the cratonic India

In the western margin of the EGP, monazite ages from aluminous granulite vary in the range ~ 1060–900 Ma which is interpreted as the time frame for metamorphism (Simmat and Raith, 2008). It was further corroborated in later studies involving monazite and zircon (Chatterjee et al., 2017b). The latter study also identified two younger metamorphic events at ~800–750 Ma and ~530–500 Ma. These authors proposed an age zonation that is characterized by the presence of ~ 950–900 Ma granulite facies metamorphism in the interior part of the EGB and the 530–500

Ma event, overprinting the granulite facies metamorphism, at the zone bordering the Bastar Craton. All the geochronological data support the model of thrusting of the EGP over the Bastar Craton at ~550-500 Ma (Gupta et al., 2000; Das et al., 2008; Biswal et al., 2007; Bhadra et al., 2004; Chatterjee et al., 2017a). In a recent study, Ravikant (2019) characterized the reworking event of the contact zone from the Bolangir area where the granulites of the EGP showed amphibolite facies metamorphism at ~500-475-Ma. Based on geochronological data (Ravikant, 2019; Ganguly et al., 2021), it can be demonstrated that the Cambrian-age metamorphism resulted from a W to NW thrusting which also reworked the Grenvillian-age older EGP crust. This Cambrian-age structural event at the northwestern tip of the EGP is correlated with the effect of far-field stress generated by the Kuunga orogen (Boger, 2011) at the margin of Australia-Mawson-Crohn craton during final assembly of the supercontinent East Gondwana. The Cambrian age thermal event described in the present study (~490 Ma) also testifies the same.

Charnockite magmatism and Proterozoic tectonics in the Rayner-Eastern Ghats mobile belt

The Rayner-Eastern Ghats (R-EG) Province is a Meso-Neoproterozoic orogenic belt resulting from the amalgamation of cratonic India and East Antarctica (Harley, 2003; Morissey et al., 2015). Petrological and high-resolution geochronological data (Mezger and Cosca, 1999; Upadhyay et al., 2009; Bose et al., 2011; Das et al., 2011; Korhonen et al., 2013; Ganguly et al., 2018) indicate that the EGP, along with the Rayner Province, formed via subduction, accretion, and collision between ca.1030-900 Ma (Dasgupta et al., 2013, 2017; Bose and Dasgupta, 2018; Ganguly et al., 2021; Bose et al. 2022). Geochronological data also suggests that the EGP underwent a prolonged rifting phase between approximately 1400-1250 Ma, marked by the emplacement of mafic and alkaline magmas (Ranjan et al., 2018). Recent evidence of felsic magmatism around ca.1230-1180 Ma at the northern part of EGP implies ensialic basement formation on top of the rifted basin (Ganguly et al., 2018; Bose et al., 2021). Sediments deposited on this basement underwent deformation and metamorphism during around ca.1180-900 Ma. The first tectonometamorphic cycle (M_1) occurred approximately 1030-990 Ma, operating in a back arc setting with crustal thinning and mantle advection. The second cycle (M_2) occurred ca.950-900 Ma and culminated in a collisional setting (Das et al., 2011; Ganguly et al., 2021; Bose et al., 2022).

In Prydz Bay and Amery Ice Shelf regions, the Rayner orogenic cycle involved three tectonic phases (Mikhalsky et al., 2018), namely the Fisher phase (ca. 1200-1100 Ma), the Beaver phase (ca. 1000-950 Ma), and the Bolingen phase (900-800 Ma). It is argued that the Rayner Province in this area experienced a two-phase collision, with an arc-continent collision at ca. 1000-970 Ma and a continent-continent collision at ca. 940-900 Ma (Kelly et al., 2002; Halpin et al., 2007; Liu et al., 2013, 2014). This history is similar to that of the EGP, but there is no clear evidence of collisional suture in this region, except for the ultramafic slabs in the Lawrence Hills and Radok Lake areas (Mikhalsky et al., 2018). The colliding arcs developed successively (Fig. 6), with back arc sedimentation, magmatism and metamorphism (Mikhalsky et al., 2006, 2018; Liu et al., 2014). Liu et al. (2014) argued that the Rayner Province and the northern part of the EGP were a single continental arc (~500 km wide) due to their similar tectonic histories. This is supported by detrital zircon age signatures and Pb isotopic compositions of K-feldspar. The Rayner Province formed due to the collision between cratonic India and cratonic East Antarctica, either in a protracted cycle, or in two pulses.

The final collision between cratonic India and East Antarctica affected the entire R-EG, causing widespread metamorphism, deformation, and magmatism. The Mawson-EGP charnockites intruded the orogenic lower crust of the R-EG in at least three different phases. The phase-1 charnockite (ca. 1145-1140 Ma) was emplaced within the Fisher arc, with no reported occurrence in the EGP at this time. The phase-2 charnockite (ca. 1080-1020 Ma) intruded the Clemens arc, and the final phase (phase-3) intruded a vast region of the Rayner-EGP arc during ca. 985-940 Ma. The charnockite and associated granitoid magmas of the EGP and Rayner Province were emplaced in a compressional orogeny when the crust was undergoing shortening (Bose et al., 2011; Ganguly et al., 2021). The collision between the R-EG and cratonic India closed the ocean basin, resulting in the present-day cratonized arc systems of R-EG punctuated by charnockite-granite arc magma. The study finds a causative relationship between the two cycles of metamorphism and intervening charnockite magmatism in a subduction-accretion-collision setting involving the Indian continent and the Rayner-EGP arc system.

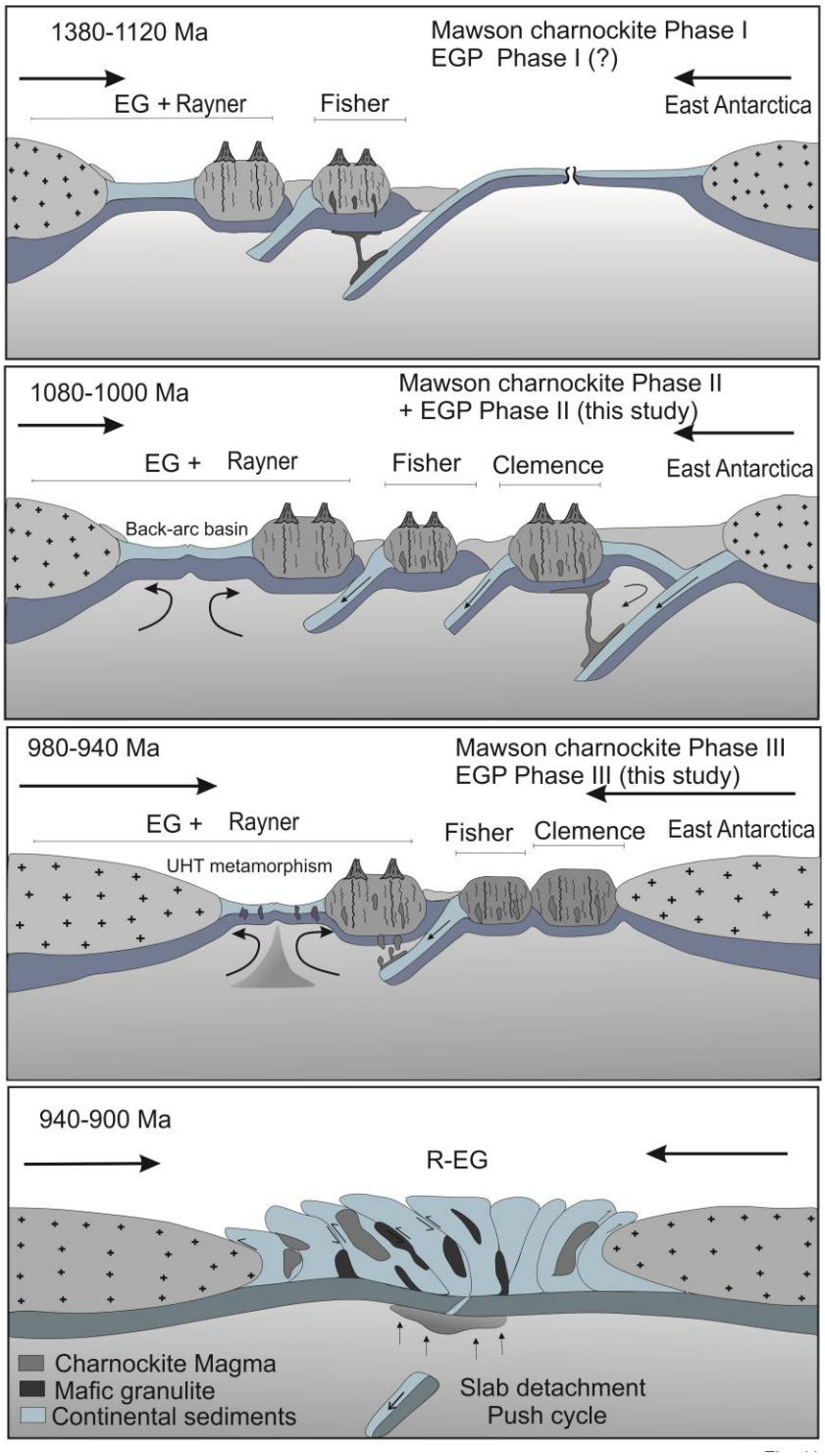

Fig. 6. Cartoon diagram showing the tectonic development between India and East Antarctica during the time span of ca. 1380-900 Ma modified after Liu et al. (2014) and Bose et al. (2022). The cartoon shows phase-wise evolution of continental/magmatic arc in the sector and crystallization of charnockite magma in the Rayner-Eastern Ghats (R-EG) orogen. See text for details.

Publications

Peer-reviewed papers

1. **Mondal, A.K**., Bose, S., Dev, J.A., Tomson, J.K., Sorcar, N. and Mukherjee, S., 2023. Petrological, geochemical and geochronological evolution of massif type charnockite from the Eastern Ghats Province, India: Implications on the regional tectonics of the Rayner-Eastern Ghats orogeny. Precambrian Research, 387, 106994.

2. **Mondal, A.K**. and Bose, S., 2019. Evolution of fluid from the ultrahigh temperature lower crust to shallower levels: Constraints from silicate–oxide–sulphide–sulphate assemblages of mafic granulites of the Eastern Ghats Belt, India. Journal of Earth System Science, 128, pp.1-28.

3. Bose, S., Ghosh, G., Kawaguchi, K., Das, K., **Mondal, A.K**. and Banerjee, A., 2021. Zircon and monazite geochronology from the Rengali-Eastern Ghats Province: Implications for the tectonic evolution of the eastern Indian terrane. Precambrian Research, 355, 106080.

4. Bose, S., **Mondal, A.K**., Bakshi, A.K. and Jose, J.R., 2020. Petrogenetic re-examination of spinel+ quartz assemblage in the Larsemann Hills, East Antarctica. Polar Science, 26, 100588.

Conference abstracts

1. **Mondal, A.K**., Sorcar, N., Bose, S., 2022. Evolution of magmatic charnockites of the Eastern Ghats Province, India and its implication on the tectonic evolution of the ca. 1000-900 Ma Rayner-Eastern Ghats orogeny. Goldschmidt conference, 14th, Hawaii, Abstract, 8964.

2. **Mondal, A.K**.., Bose, S., 2022. Characterization of lower crustal fluid using oxide-silicate-sulphide assemblages of mafic granulite from the Eastern Ghats Belt, India. International Geological Congress, 36th, India, Abstract, 722-532.

References

Abati, J., Arenas, R., Catalan, J.R.M., Garcia, F.D., 2003 Anticlockwise P–T path of granulites from the Monte Castelo gabbro (Ordenes Complex, NW Spain). J. Petrol. 44, 305–327.

Aftalion, M., Bowes, D.R., Dash, B., Dempster, T.J., 1988. Late Proterozoic charnockites in Orissa, India: A U-Pb and Rb-Sr isotopic study. J. Geol. 96, 663–676.

Andersen, D.J., Lindsley, D.H., Davidson, P.M., 1993. QUILF: A pascal program to assess equilibria among Fe-Mg-Mn-Ti oxides, pyroxenes, olivine, and quartz. Comp. Geosci. 19, 1333–1350.

Barnes, J.D., Manning, C.E., Scambelluri, M., Selverstone, J., 2018. The behavior of halogens during subduction-zone processes; In: The role of halogens in terrestrial and extraterrestrial geochemical processes: Surface, crust, and mantle (eds) Harlov D E and Aranovich L, Springer, Berlin, Geochemistry Chapter, Vol. 8, pp. 545–590.

Beard, J.S., Lofgren, G.E., 1991. Dehydration melting and water-saturated melting of basaltic and andesitic greenstones and amphibolites at 1, 3, and 6. 9 kbar. J. Petrol. 32, 365–401.

Belousova, E.A., Griffin, W.L., O'Reilly, S.Y., Fisher, N.L., 2002. Igneous zircon: trace element composition as an indicator of source rock type. Contrib. Mineral. Petrol. 143, 602−622.

Bhadra, S., Gupta, S., Banerjee, M., 2004. Structural evolution across the Eastern Ghats Mobile Belt-Bastar craton boundary, India: hot over cold thrusting in an ancient collision zone. J. Struct. Geol. 26, 233-245.

Bhui, U.K., Sengupta, P., Sengupta, P., 2007. Phase relations in mafic dykes and their host rocks from Kondapalle, Andhra Pradesh, India: Implications for the time–depth trajectory of the Palaeoproterozoic (late Archaean?) granulites from southern Eastern Ghats Belt. Precamb. Res. 156, 153–174.

Biswal, T.K., De Waele, B., Ahuja, H., 2007. Timing and dynamics of the juxtaposition of the Eastern Ghats Mobile Belt against the Bhandara Craton, India: a structural and zircon U-Pb SHRIMP study of the fold-thrust belt and associated nepheline syenite plutons. Tectonics 26 (4).

Bose, S., 2020. Geology of the Proterozoic Eastern Ghats Belt: recent developments and outstanding issues. In: (Eds. Banerjee, D.M., Jain, A.K., Dasgupta, S., Bajpai, S.) Special issue of the Proc. Ind. Nat. Sci. Acad. 36th IGC 2020 Geoscience Research in India: The Indian Report to IUGS 2016-2020, 86, 87–97.

Bose, S, Dasgupta, S., 2018. Eastern Ghats Belt, Grenvillian-age tectonics and the evolution of the Greater Indian Landmass: a critical perspective. J. Ind. Inst. Sci. 98, 345−363.

Bose, S., Das, K., Fukuoka, M., 2005. Fluorine content of biotite in granulite-grade metapelitic assemblages and its implications for the Eastern Ghats granulites. Eur. J. Mineral. 17, 665–674.

Bose, S., Ghosh, G., Kawaguchi, K., Das, K., Mondal, A.K., Banerjee, A., 2021. Zircon and monazite geochronology from the Rengali-Eastern Ghats Province: Implications for the tectonic evolution of the eastern Indian terrane. Precambr. Res. 355, 106080.

Bose S, Fukuoka M, Sengupta P and Dasgupta S 2000 Evolution of high-Mg-Al granulites from sunkarametta, Eastern Ghats, India: Evidence for a lower crustal heating-cooling trajectory; J. Metamorph. Geol. 18 223–240.

Bose, S., Pal, S., Fukuoka, M., 2003. Pressure–temperature-fluid evolutionary history of orthopyroxene-bearing quartzofeldspathic and mafic granulites from northern parts of the Eastern Ghats Belt, India: implications for Indo-Antarctic correlation. J. Asian Earth Sci. 22, 81–100.

Bose, S., Das, K., Torimoto, J., Dunkley, D.J., 2020. Origin of orthopyroxene-bearing felsic gneiss in the perspective of ultrahigh temperature metamorphism: an example from the Chilka Lake migmatite complex, Eastern Ghats Belt, India. Mineral. Mag. 84, 712−737.

Bose, S., Das, K., Torimoto, J., Arima, M., Dunkley, D.J., 2016. Evolution of the Chilka Lake granulite complex, northern Eastern Ghats Belt, India: evidence of ~ 780 Ma decompression of the deep crust and its implication on the India-Antarctica correlation. Lithos 263, 161–189.

Bose, S., Dunkley, D.J., Dasgupta, S., Das, K., Arima, M., 2011. India-Antarctica-Australia-Laurentia connection in the Paleo-Mesoproterozoic revisited: Evidence from new zircon U-Pb and monazite chemical age data from the Eastern Ghats Belt, India. Geol. Soc. Amer. Bull. 123, 2031–2049.

Bose, S., Das, K., Ohnishi, I., Torimoto, J., Karmakar, S., Shinoda, K., Dasgupta, S., 2009. Characterization of oxide assemblages of a suite of granulites from Eastern Ghats Belt, India: Implication to the evolution of C–O–H–F fluids during retrogression. Lithos 113, 483–497.

Bose, S., Sorcar, N., Das, K., Ganguly, P., 2022. Pulsed tectonic evolution in long-lived orogenic belts: an example from the Eastern Ghats Belt, India. Precambr. Res. 369, 106522.

Boger, S.D., 2011. Antarctica - before and after Gondwana. Gondwana Res. 19, 335–371.

Brown, M., 1994. The generation, segregation, ascent and emplacement of granite magma: the migmatite-to-crustally-derived granite connection in thickened orogens. Earth Sci. Rev. 36, 83–130.

Condie, K.C., 2005. TTGs and adakites: are they both slab melts? Lithos, 80, 33-44.

Chatterjee, A., Das, K., Bose, S., Hidaka, H., 2017a. Age-integrated tectonic evolution across the orogen-craton boundary: age zonation and shallow-to deep crustal participation during Late Cambrian cratonisation of Eastern Ghats Belts, India. Lithos 290–291, 269–293.

Chatterjee, A., Das, K., Bose, S., Ganguly, P., Hidaka, H., 2017b. Zircon U-Pb SHRIMP and monazite EPMA U-Th-total Pb geochronology of granulites of the western boundary, Eastern Ghats Belt, India: New possibility for Neoproterozoic exhumation history. In: Dasgupta, S., Pant, N.C. (Eds.), Crustal Evolution of India and Antarctica: The Supercontinent Connection. Geol. Soc. Lond. Spec. Pub. 457, pp. 105–140.

Crawford, M., Hollister, L., 1986. Metamorphic fluids: the evidence from fluid inclusions. Fluid-Rock Interactions during Metamorphism, Springer New York NY: 1–35.

Das, K., Bose, S., Torimoto, J., Hayasaka, Y., Dunkley, D., 2021. Tracking C-O-H fluid-rock interactions in reworked UHT granulite: Tectonic evolution from ca. 990 Ma to ca. 500 Ma in orogenic interior of Eastern Ghats Belt, India. Lithos 398, 106287.

Das, K., Bose, S., Karmakar, S., Dunkley, D.J., Dasgupta, S., 2011. Multiple tectonometamorphic imprints in the lower crust: first evidence of c. 950 Ma compressional reworking of older UHT metamorphosed aluminous granulites from the Eastern Ghats Belt, India. Geol. J. 46, 217–239.

Das, S., Nasipuri, P., Bhattacharya, A., Swaminathan, S., 2008. The thrust-contact between the Eastern Ghats Belt and the adjoining Bastar craton (Eastern India): evidence from mafic granulites and tectonic implications. Precambr. Res. 162, 7085.

Das, K., Tomioka, N., Bose, S., Ando, J., Ohnishi, I., 2017. The occurrence of fluor-wagnerite in UHT granulites and its implications towards understanding fluid regimes in the evolution of deep crust: a case study from the Eastern Ghats Belt, India. Mineral. Petrol. 111, 417–429.

Dasgupta, S., Bose, S., Bhowmik, S.K., Sengupta, P., 2017. Eastern Ghats Belt, India in the context of supercontinent assembly. In: Pant, N.C., Dasgupta, S. (Eds.) Crustal Evolution of India and Antarctica: the supercontinent connection. Geol. Soc. Lond. Spec. Pub. 457, pp. 87−104.

Dasgupta, S., Bose, S., Das, K., 2013. Tectonic evolution of the Eastern Ghats Belt. Precambr. Res. 227, 247−258.

Dasgupta, S., Sengupta, P., Fukuoka, M., Bhattacharya, P.K., 1991. Mafic granulites from the Eastern Ghats, India: further evidence for extremely high temperature crustal metamorphism. J. Geol. 99, 124−133.

Dasgupta, S., Sengupta, P., Mondal, A., Fukuoka, M., 1993. Mineral chemistry and reaction textures in metabasites from the Eastern Ghats belt, India and their implications. Mineral. Mag. 57, 113–120.

Dobmeier, C., Raith, M., 2003. Crustal architecture and evolution of the Eastern Ghats Belt and adjacent regions of India. In: Yoshida, M., Windley, B.F., Dasgupta, S. (Eds.), Proterozoic East Gondwana: supercontinent assembly and breakup. Geol. Soc. Lond. Spec. Pub. 206, pp. 145−168.

Duchesne, J.C., Wilmart, E., 1997. Igneous charnockites and related rocks from the Bjerkreim–Sokndal layered intrusion (Southwest Norway): a jotunite (hypersthene monzodiorite)-derived A-type granitoid suite. J. Petrol. 38, 337−369.

Duchesne, J.C., Wilmart, E., Demaiffe, D., Hertogen, J., 1989. Monzonorites from Rogaland (Southwest Norway): a series of rocks coeval but not comagmatic with massif-type anorthosites. Precambr. Res. 45, 111−128.

Dziggel, A., Diener, J.F.A., Stoltz, N.B., Kolb, J., 2012. Role of H_2O in the formation of garnet coronas during near-isobaric cooling of mafic granulites: the Tasiusarsuaq terrane, southern West Greenland. J. Metamorph. Geol. 30, 957–972.

Emslie, R.F., Hamilton, M.A., Thériault, R.J., 1994. Petrogenesis of a mid-Proterozoic anorthosite-mangerite-charnockite-granite (AMCG) complex: Isotopic and chemical evidence from the Nain Plutonic Suite. J. Geol. 102, 539−558.

Feisel, Y., White, R.W., Palin, R.M., 2018. New constraints on granulite-facies metamorphism and melt production in the Lewisian Complex, northwest Scotland. J. Metamorph. Geol. doi: 10.1111/jmg.12311.

Ferry, J.M., Watson, E.B., 2007. New thermodynamic models and revised calibrations for the Ti-in-zircon and Zr-in-rutile thermometers. Contrib. Mineral. Petrol. 154, 429−437.

Frost, B.R., 1991. Introduction to oxygen fugacity and its petrologic importance. Rev. Mineral. Geochem. 25, 1–9.

Frost, B.R., Chacko, T., 1989. The granulite uncertainty principle: limitations on thermobarometry in granulites. J. Geol. 97, 435–450.

Frost, B.R., Frost, C.D., (2008). On charnockites. Gond. Res. 13, 30–44.

Frost, B.R., Frost, C.D., Hulsebosch, T.P., Swapp, S.M., 2000. Origin of the charnockites of the Louis lake Batholith, wind River Range, Wyoming. J. Petrol. 41, 1759–1776.

Ganguly, P., Ghosh, G., Bose, S. Das, K., 2021. Polyphase deformation and ultrahigh temperature metamorphism of the deep continental crust: Implications for tectonic evolution of the northern Eastern Ghats Belt, India. J. Struct. Geol. 143, 104250.

Ganguly, P., Das, K., Bose, S., Ghosh, G., Hayasaka, Y., Hidaka, H., 2018. U-Pb zircon and U-Th-total Pb monazite ages from the Phulbani Domain of the Eastern Ghats Belt, India: Time constraints on high-grade metamorphism and magmatism in the lower crust. Precambr. Res. 316, 1–23.

Ganguly, P., Bose, S., Das, K., Torimoto, J., Ghosh, G., 2017. Origin of spinel + quartz assemblage in a Si-undersaturated ultrahigh temperature aluminous granulite and its implication in the P-T-fluid history of the Phulbani domain, Eastern Ghats Belt, India. J. Petrol. 58, 1941–1974.

Gao, P., Santosh, M., Yang, C.X., Kwon, S., Ramkumar, M., 2021. High Ba–Sr adakitic charnockite suite from the Nagercoil Block, southern India: Vestiges of Paleoproterozoic arc and implications for Columbia to Gondwana. Geosci. Front. 12, 101126.

Grew, E.S., Manton, W.I., 1986. A new correlation of sapphirine granulites in the Indo-Antarctic metamorphic terrain: Late Proterozoic dates from the Eastern Ghats province of India. Precambr. Res. 33, 123–137.

Grimes, C.B., Wooden, J.L., Cheadle, M.J., John, B.E. 2015. “Fingerprinting” tectonomagmatic provenance using trace elements in igneous zircon. Contrib. Mineral. Petrol. 170, 46.

Grimes, C.B., John, B.E., Kelemen, P.B., Mazdab, F.K., Wooden, J.L., Cheadle, M.J., Hanghøj, K., Schwartz, J.J., 2007. The trace element chemistry of zircons from oceanic crust: a method for distinguishing detrital zircon provenance. Geology 35, 643–646.

Gupta, S., Bhattacharya, A., Raith, M., Nanda, J.K., 2000. Pressure-temperature-deformational history across a vestigial craton -mobile belt boundary: the western margin of the Eastern Ghats Belt at Deobhog. India. J. Metamorph. Geol. 18, 683-697.

Halpin, J.A., Daczko, N.R., Milan, L.A., Clarke, G.L., 2012. Decoding near-concordant U–Pb zircon ages spanning several hundred million years: recrystallisation, metamictisation or diffusion? Contrib. Mineral. Petrol. 163, 67–85.

Halpin, J.A., Clarke, G.L., White, R.W., Kelsey, D.E., 2007. Contrasting P–T–t paths for Neoproterozoic metamorphism in MacRobertson and Kemp Lands, east Antarctica. J. Metamorph. Geol. 25, 683–701.

Harley, S.L., 2008. Refining the P–T records of UHT crustal metamorphism. J. Metamorph. Geol. 26, 125–154.

Harley, S.L., 2003. Archaean–Cambrian development of East Antarctica: metamorphic characteristics and tectonic implications. In: Yoshida, M., Windley, B.F., Dasgupta, S. (Eds.), Proterozoic East Gondwana: supercontinent assembly and breakup. Geol. Soc. Lond. Spec. Pub. 206, pp. 203–230.

Harlov D E 2012 The potential role of fluids during regional granulite-facies dehydration in the lower crust; Geosci. Front. 3 813–827.

Harlov, D., Newton, R.C., Hansen, E.C., 1997. Oxide and sulphide minerals in highly oxidized, Rb-depleted, Archaean granulites of the Shevaroy Hills Massif, South India: Oxidation states and the role of metamorphic fluids. J. Metamorph. Geol. 15, 701–717.

Harlov, D.E., Van Den Kerkhof, A., Johansson, L., 2013. The Varberg–Torpa charnockite–granite association, SW Sweden: mineralogy, petrology, and fluid inclusion chemistry. J. Petrol. 54, 3–40.

Hollocher, K., Robinson, P., Walsh, E., Roberts, D., 2012. Geochemistry of amphibolite-facies volcanics and gabbros of the Støren Nappe in extensions west and southwest of Trondheim, Western Gneiss Region, Norway: a key to correlations and paleotectonic settings. Am. J. Sci. 312, 357–416.

Hoskin, P.W.O., Black, L.P., 2002. Metamorphic zircon formation by solid-state recrystallization of protolith igneous zircon. J. Metamorph. Geol. 18, 423–439.

Hughes, S.S., Lewis, S.E., Bartholomew, M.J., Sinha, A.K., Herz, N., Tollo, R.P., Corriveau, L., McLelland, J.M., Bartholomew, M.J., 2004. Geology and geochemistry of granitic and charnockitic rocks in the central Lovingston massif of the Grenvillian Blue Ridge terrane. Mem. Geol. Soc. Am. 549–570.

Huppert, H.E., Sparks, R.S.J., 1988. The generation of granitic magmas by intrusion of basalt into continental crust. J. Petrol. 29, 599-624.

Keppler, H., 1996. Constraints from partitioning experiments on the composition of subduction-zone fluids. Nature 380, 237–240.

Kelly, N.M., Clarke, G.L., Fanning, C.M., 2002. A two-stage evolution of the Neoproterozoic Rayner Structural Episode: new U–Pb sensitive high resolution ion microprobe constraints from the Oygarden Group, Kemp Land, East Antarctica. Precambr. Res. 116, 307–330.

Kelsey, D.E., Morrissey, L.J., Hand, M., Clark, C., Tamblyn, R., Gaehl, A.A., Marshall, S., 2017. Significance of post-peak metamorphic reaction microstructures in the ultrahigh temperature Eastern Ghats Province, India. J. Metamorph. Geol. 35, 1081–1109.

Kilpatrick, J.A., Ellis, D.J., 1992. C-type magmas: igneous charnockites and their extrusive equivalents. Earth Env. Sci. Trans. Royal Soc. Edin. 83, 155−164.

Klaver, M., de Roever, E.W., Nanne, J.A., Mason, P.R., Davies, G.R., 2015. Charnockites and UHT metamorphism in the Bakhuis Granulite Belt, western Suriname: Evidence for two separate UHT events. Precambr. Res. 262, 1−19.

Korhonen, F.J., Clark, C., Brown, M., Bhattacharya, S., Taylor, R., 2013. How long-lived is ultrahigh temperature (UHT) metamorphism? Constraints from zircon and monazite geochronology in the Eastern Ghats orogenic belt, India. Precambr. Res. 234, 322−350.

Korhonen, F.J., Clark, C., Brown, M., Bhattacharya, S., Taylor, R., 2013b. How long-lived is ultrahigh temperature (UHT) metamorphism? Constraints from zircon and monazite geochronology in the Eastern Ghats orogenic belt, India. Precambr. Res. 234: 322–350.

Krause, O., Dobmeier, C., Raith, M.M., Mezger, K., 2001. Age of emplacement of massif-type anorthosites in the Eastern Ghats Belt, India: constraints from U-Pb zircon dating and structural studies. Precambr. Res. 109, 25−38.

Kullerud, G., 1957. Phase relations in the Fe-SO system. Carnegie Institute of Washington Year Book 56, 198–200.

Liu, X.C., Jang, B.-M., Zhao, Y., Liu, J., Ren, L.D. 2014. Geochemistry and geochronology of Mesoproterozoic basement rocks from the eastern Amery Ice Shelf and southwestern Prydz Bay, East Antarctica: implications for a long-lived magmatic accretion in a continental arc. Am. J. Sci. 314, 508−547.

Liu, X.C., Zhao, Y., Hu, J. M. 2013. The c. 1000–900 Ma and c. 550–500 Ma tectonothermal events in the Prince Charles Mountains-Prydz Bay region, East Antarctica, and their relations to supercontinent evolution. In: Harley, S.L., Fitzsimons, I.C.W., Zhao, Y. (Eds.), Antarctica and Supercontinent Evolution. Geol. Soc. Lond. Spec. Pub. 383, pp. 95–112.

López, S., Castro, A., 2001. Determination of the fluid–absent solidus and supersolidus phase relationships of MORB-derived amphibolites in the range 4–14 kbar. Am. Mineral. 86, 1396–1403.

Manning, C.E., 2004. The chemistry of subduction-zone fluids. Earth Planet. Sci. Lett. 223, 1-6.

Manning, C., Aranovich, L., 2014. Brines at high pressure and temperature: thermodynamic, petrologic and geochemical effects. Precambr. Res., 253, 6–16.

McDonough, W.F., Sun, S.S., 1995. The composition of the Earth. Chem. Geol. 120, 223−253.

Mendes, J.C., De Campos, C.M., 2012. Norite and charnockites from the Venda Nova Pluton, SE Brazil: Intensive parameters and some petrogenetic constraints. Geosci. Front. 3, 789−800.

Mezger, K., Cosca, M.A., 1999. The thermal history of the Eastern Ghats Belt (India) as revealed by U-Pb and $^{40}Ar/^{39}Ar$ dating of metamorphic and magmatic minerals: implications for the SWEAT correlation. Precambr. Res. 94, 251–271.

Mikhalsky, E.V., Leitchenkov, G.L., Kiselev, A.V., Popov, S.V., Vorobiev, D.M., 2018. Explanatory notes to geological map of Mac Robertson Land, Princess Elizabeth Land, and Prydz Bay (East Antarctica) scale 1:1 000000. In: Mikhalsky, E.V., Leitchenkov. G.L., SPb.: FSBI "VNIIOkeangeologia", 82 p.

Mikhalsky, E.V., Sheraton, J.W., Hahne, K., 2006. Charnockite Composition in relation to the Tectonic Evolution of East Antarctica. Gond. Res. 9, 379–397.

Mohan, A., Sachan, H.K., Singh, P.K., 2003. High-density carbonic fluid inclusions in charnockites from Eastern Ghats, India: petrologic implications. J. Asian Earth Sci. 22, 101–113.

Möller, P., Weise, S.M., Althaus, E., Bach, W., Behr, H.J., Borchardt, R., Bräuer, K., Drescher, J., Erzinger, J., Faber, E., Hansen, B.T., Horn, E.E., Huenges, E., Kämpf, H,, Kessels, W., Kirsten, T., 1997. Paleofluids and recent fluids in the upper continental crust: Results from the German Continental Deep Drilling Program (KTB). J. Geophys. Res. Solid Earth 102, 18233–18254.

Morrissey, L.J., Hand, M., Kelsey, D.E., 2015. Multi-stage metamorphism in the Rayner-Eastern Ghats Terrane: P-T-t constraints from the northern Prince Charles Mountains, east Antarctica. Precambr. Res. 267, 137–163.

Newton, R.C., Manning, C.E., 2005. Solubility of anhydrite, $CaSO_4$, in $NaCl–H_2O$ solutions at high pressures and temperatures: applications to fluid–rock interaction. J. Petrol. 46: 701–716.

Newton, R.C., Smith, J.V., Windley, B.F., 1980. Carbonic metamorphism, granulites and crustal growth. Nature 288, 45–50.

Ni, H., Zhang, L., Xiong, X., Mao, Z., Wang, J., 2017. Supercritical fluids at subduction zones: Evidence, formation condition, and physicochemical properties; Earth Sci. Rev. 167 62–71.

PatiñoDouce, A.E., Beard, J.S., 1995. Dehydration-melting of biotite gneiss and quartz amphibolite from 3 to 15 kbar. J. Petrol. 36, 707–738.

Paul, D.K., Barman, T.R., McNaughton, N.J., Fletcher, I.R., Potts, P.J., Ramakrishnan, M., Augustine, P.F., 1990. Archean-Proterozoic evolution of Indian charnockites: isotopic and geochemical evidence from granulites of the Eastern Ghats Belt. J. Geol. 98, 253-263.

Percival, J.A., Mortensen, J.K., 2002. Water-deficient calc-alkaline plutonic rocks of northeastern Superior Province, Canada: significance of charnockitic magmatism. J. Petrol. 43, 1617–1650.

Rajesh, H.M., Santosh, M., Wan, Y., Liu, D., Liu, S.J., Belyanin, G.A., 2014. Ultrahigh temperature granulites and magnesian charnockites: evidence for Neoarchean accretion along the northern margin of the Kaapvaal Craton. Precambr. Res. 246, 150–159.

Ramakrishnan, M., Nanda, J.K., Augustine, P., 1998. Geological evolution of the Proterozoic Eastern Ghats mobile belt. In: Ramakrishnan, M., Paul, D.K., Mishra, R.N. (Eds.), Geological evolution of Proterozoic Eastern Ghats Mobile Belt. Geol. Surv. Ind. Spec. Pub. 44, 1–21.

Ranjan, S., Upadhyay, D., Abhinay, K., Pruseth, K.L., Nanda, J.K., 2018. Zircon geochronology of deformed alkaline rocks along the Eastern Ghats Belt margin: India–Antarctica connection and the Enderbia continent. Precambr. Res. 310, 407–424.

Ravikant, V., 2019. Cambrian garnet Sm-Nd isotopic ages from the polydeformed Bolangir anorthosite complex, Eastern Ghats Belt, India: implications for intraplate orogeny coeval with Kuunga orogeny during Gondwana assembly. J. Geol. 127, 437456.

Rickers, K., Mezger, K., Raith, M.M., 2001. Evolution of the continental crust in the Proterozoic Eastern Ghats Belt, India and new constraints for Rodinia reconstruction: implications from Sm–Nd, Rb–Sr and Pb–Pb isotopes. Precambr. Res. 112, 183–210.

Rollinson, H.R., 1980. Iron-titanium oxides as an indicator of the role of the fluid phase during the cooling of granites metamorphosed to granulite grade. Mineral. Mag. 43, 623–631.

Rushmer, T., 1991. Partial melting of two amphibolites: contrasting experimental results under fluid-absent conditions. Contrib. Mineral. Petrol. 107, 41–59.

Sarkar, S., Santosh, M., Dasgupta, S., Fukuoka, M., 2003. Very high density CO_2 associated with ultrahigh-temperature metamorphism in the Eastern Ghats granulite belt, India. Geology 31, 51–54.

Sarkar, T., Schenk, V., Berndt, J., 2015. Formation and evolution of a Proterozoic magmatic arc: geochemical and geochronological constraints from meta-igneous rocks of the Ongole domain, Eastern Ghats Belt, India. Contrib. Mineral. Petrol. 169, 1–27.

Schorn, S., Diener, J.F., Sorger, D., Clark, C., 2020. The contribution of charnockite magmatism to achieve near-ultrahigh temperatures in the Namaqua–Natal Metamorphic Province, South Africa. Lithos 368, 105585.

Sengupta, P., Dasgupta, S., Bhui, U.K., Ehl, J., Fukuoka, M., 1996. Magmatic evolution of mafic granulites from Anakapalle, Eastern Ghats, India: implications for tectonic setting of a Precambrian high-grade terrain. J. Southeast Asian Earth Sci. 14, 185–198.

Shaw, R.K., Arima, M., Kagami, H., Fanning, C.M., Shiraishi, K., Motoyoshi, Y., 1997. Proterozoic events in the Eastern Ghats granulite belt, India: evidence from Rb-Sr, Sm-Nd systematics, and SHRIMP dating. J. Geol. 105, 645–656.

Simmat, R., Raith, M., 2008. U-Th–Pb monazite geochronometry of the Eastern Ghats Belt, India: timing and spatial disposition of poly-metamorphism. Precambr. Res. 162, 16–39.

Sun, S.S., McDonough, W.F., 1989. Chemical and isotopic systematics of oceanic basalts: implications for mantle composition and processes. In: Saunders, A.D., Norry, M.J. (Eds.) Magmatism in the Ocean Basins, Geol. Soc. Lond. Spec. Pub. 42, 313–345.

Stober, I., Bucher, K., 2005. The upper continental crust, an aquifer and its fluid: hydaulic and chemical data from 4 km depth in fractured crystalline basement rocks at the KTB test site. Geofluids 5, 8–19.

Tomson, J.K., Rao, Y.B., Kumar, T.V., Choudhary, A.K., 2013. Geochemistry and neodymium model ages of Precambrian charnockites, Southern Granulite Terrain, India: Constraints on terrain assembly. Precambr. Res. 227, 295–315.

Tomson, J.K., Rao, Y.B., Kumar, T.V., Rao, J.M., 2006. Charnockite genesis across the Archaean–Proterozoic terrane boundary in the South Indian Granulite Terrain: Constraints from major–trace element geochemistry and Sr–Nd isotopic systematics. Gond. Res. 10, 115–127.

Touret, J.L., 1985. Fluid regime in southern Norway: the record of fluid inclusions. The deep Proterozoic crust in the north Atlantic provinces, Springer, Dordrecht: 517–549.

Upadhyay, D., 2008. Alkaline magmatism along the southeastern margin of the Indian shield: implications for regional geodynamics and constraints on craton–Eastern Ghats Belt suturing. Precamb. Res. 162, 59–69.

Upadhyay, D., Gerdes, A., Raith, M.M., 2009. Unraveling sedimentary provenance and tectonothermal history of high-temperature metapelites, using zircon and monazite chemistry: a case study from the Eastern Ghats Belt, India. J. Geol. 117, 665–683.

Villaseca, C., Orejana, D., Higueras, P., Pérez-Soba, C., Serrano, J.G. and Lorenzo, S., 2022. The evolution of the subcontinental mantle beneath the Central Iberian Zone: Geochemical tracking of its mafic magmatism from the Neoproterozoic to the Cenozoic. Earth-Sci. Rev. 228, p.103997.

Watson, E.B., Brenan, J.M., 1987. Fluids in the lithosphere, 1. Experimentally-determined wetting characteristics of CO_2-H_2O fluids and their implications for fluid transport, host-rock physical properties, and fluid inclusion formation. Earth and Planet. Sci. Let. 85: 497–515.

Yang, Q.Y., Santosh, M., 2015. Charnockite magmatism during a transitional phase: implications for late Paleoproterozoic ridge subduction in the North China Craton. Precambr. Res. 261, 188–216.

Yang, Q.Y., Santosh, M., Collins, A.S., Teng, X.M., 2016. Microblock amalgamation in the North China Craton: Evidence from Neoarchaean magmatic suite in the western margin of the Jiaoliao Block. Gond. Res. 31, 96–123.

Young, D.N., Zhao, J.X., Ellis, D.J., McCulloch, M.T., 1997. Geochemical and Sr-Nd isotopic mapping of source provinces for the Mawson charnockites, east Antarctica: implications for Proterozoic tectonics and Gondwana reconstruction. Precambr. Res. 86, 1–19.

Zheng, Y.F., Chen, Y.X., 2016. Continental versus oceanic subduction zones. Nat. Sci. Rev. 3, 495-519.